



# Measurement of Minor Element Distributions in Complex Copper Converting Slags Using Quantitative Microanalysis Techniques

JIANG CHEN,<sup>1,5</sup> ATA FALLAH-MEHRJARDI,<sup>2,3</sup> ANDREAS SPECHT,<sup>3</sup>  
and HUGH ST.C. O'NEILL<sup>4</sup>

1.—Centre for Advanced Microscopy, The Australian National University, Acton, Australia.  
2.—Vesuvius, Belgium. 3.—Research and Development, Aurubis AG, Hamburg, Germany.  
4.—School of Earth, Atmosphere and Environment, Monash University, Clayton, Australia.  
5.—e-mail: jcanu2018@gmail.com

The distribution coefficients of minor elements Co, Ni, Zn, Pb, Bi, Sn, Sb, As, Te, Se, Ga, Ge, and In between slag, matte, and spinel phases in industrial copper converting slag samples have been determined by the microanalysis method using the combination of electron probe microanalysis (EPMA) with laser-ablation inductively coupled plasma mass spectrometry (LA-ICP-MS). The major factors affecting analysis accuracy, including analysis precision, detection limits, background correction, beam damage, and standard selection, are discussed. The determined minor elements distributions show good consistency with most recently published literature data. The present study demonstrates that minor element distributions with precision close to that of controlled laboratory studies could be obtained by direct measurement of plant samples upon careful sampling, microstructural examination, and the application of customized analytical routines. The advantages and limitations of using microanalysis techniques for industry slag assay are also discussed.

## INTRODUCTION

Current primary copper production via the pyrometallurgical route typically involves smelting of copper sulfide ore concentrate to produce copper matte, which is then converted to blister copper by removing impurities in the form of slag (e.g., Fe, Pb, and Zn) and gas (mainly SO<sub>2</sub>). Careful control of the distribution of minor elements during the process has been of ongoing interest to copper producers because of both economical and environmental considerations. Harmful elements such as As and Pb must be removed from the matte/metal and transferred to the slag, where they can be disposed of, while valuable elements such as Ni, Au, and Ag should be reserved in the matte/metal phase for subsequent recovery.

Conventionally, the minor element departments in smelting/converting products, namely slag, matte, copper metal, and flue dust, are determined by x-ray fluorescence (XRF) and/or solution inductively coupled plasma optical emission spectroscopy (ICP-OES)/atomic emission spectroscopy (AES)/mass spectrometry (MS). However, at industrial sites, these materials are often cross-contaminated due to crude sampling procedures and incomplete phase separation, e.g., finely suspended Cu matte particles in slag phase. Therefore, such bulk chemical analysis methods are often incapable of delivering accurate information on the minor element distributions.

With the development and application of a variety of microanalysis techniques, including electron microprobe x-ray analysis (EPMA) and laser-ablation inductively coupled plasma mass spectrometry (LA-ICP-MS), *in situ* quantitative measurement of chemical compositions of both crystalline and amorphous phases has become possible. The major advantage of these microanalysis techniques is that

sampling is carried out on an area of 1  $\mu\text{m}$  to 100  $\mu\text{m}$  in the region of interest, so that contamination from mixing of phases is avoided, or at least minimized. Among the microanalysis techniques that are readily available, LA-ICP-MS<sup>1</sup> is becoming widely used for trace elements (< 0.1 wt.% or 1000 ppm) due to its superior detection limit for most elements (sub-ppm). However, there are a number of issues associated with LA-ICP-MS that have limited its applicability to metallurgy research. In particular, its analytical accuracy relies heavily on the use of matrix-matched standards, but the availability of sulfide and metal standards is at present limited. Secondly, the poor spatial resolution (> 20  $\mu\text{m}$ ) relative to EPMA ( $\sim$  1  $\mu\text{m}$  to 2  $\mu\text{m}$ ) makes measurement of small features correspondingly challenging. Notwithstanding its superior spatial resolution, EPMA has often been perceived as reliable only for major elements (> 1 wt.%). In fact, recent advances in EPMA instrumentation such as the field-emission electron gun, large-size diffraction crystals, and automation of aggregated intensity from multiple spectrometers have made it feasible to use EPMA to measure at least the more abundant trace elements (> 100 ppm) on a routine basis.

Previously, Avarmaa et al.<sup>2</sup> studied the equilibrium distribution of the precious metals Au, Ag, Pd, Rh, and Pt between iron silicate slag and copper matte at SiO<sub>2</sub> saturation at 1250 °C to 1350 °C using high-temperature equilibration, rapid quenching, and microanalysis techniques. The authors determined distribution coefficients by measuring the precious metals in the slag and matte phase at very low levels (down to  $\sim$  1 ppm) by combining EPMA and LA-ICP-MS.

Shishin et al.<sup>3–5</sup> experimentally determined the distribution of various minor elements including Ag, Au, As, Sn, and Sb between slag, matte, and copper metal phase under equilibrium conditions relevant to the copper smelting/converting process using experimental and analysis methods similar to those of Avarmaa et al.<sup>2</sup> The studies resolved the significant discrepancies in minor element distribution coefficients found in literature data, which were mostly determined by bulk chemical analysis methods.

While quantitative microanalysis techniques have been successfully applied to study minor element distributions at the laboratory scale, examples of their direct application to industry samples have rarely been reported. In this study, we determined distribution coefficients of minor elements Co, Ni, Zn, Pb, Bi, Sn, Sb, As, Te, Se, Ga, Ge, and In during an industrial copper converting process between slag, matte, and spinel phase by combining EPMA with LA-ICP-MS. In particular, we focused on developing a suitable analytical routine to address the complex nature of the samples.

## EXPERIMENTAL PROCEDURES

### Sampling

The copper converting process involves two major steps: the slag blow and the copper blow. During the slag blow, air (or oxygen-enriched air) is injected via submerged tuyeres in the Pierce–Smith converter (PSC) to oxidize Fe and S from the molten matte, taken from a flash smelting furnace (FSF). This produces white metal (having approximately 77 wt.% to 78 wt.% Cu). Silica flux is added continuously during the oxidation process to form the slag phase. At the end of the slag blow step, slag is tapped. During the copper blow step, most of the remaining S and other impurities in the white metal are then removed by further air injection, and blister Cu is formed (Cu > 98.5 wt.%).

In this study, slag samples were collected from the PSC of a primary copper production process at different stages during the slag blow step. A pre-heated spoon was used to collect slag samples at tapping, which were then quickly poured into cold water to preserve the phase assemblage at high temperature. The sampling temperature was estimated to be between 1250 °C and 1350 °C. The concentration of major elements of an industrial PSC slag determined by XRF is presented in Supplementary Table S1.

### Analytical Setup

#### EPMA

A small fraction of randomly selected granules of each sample was mounted in epoxy resin and ground/polished using conventional metallography methods. A 20-nm-thick C coating was applied to the polished sample surface. Microstructure examination and quantitative elemental analysis were performed on the slag samples using a JEOL 8530F Plus field-emission electron microprobe at the Centre for Advanced Microscopy, Australian National University. The x-ray emission lines used for analysis and the standards used for calibration are presented in Supplementary Table S2. To determine the major and minor elements (> 0.5 wt.%) in all phases, an acceleration voltage of 20 keV and a probe current of 20 nA were used; for trace elements (< 0.5 wt.%), a probe current of 100 nA for matte and 150 nA for slag and spinel were used. Spot size was 5  $\mu\text{m}$  for spinel and 30  $\mu\text{m}$  for slag and matte.

Unlike the synthetic experimental samples produced in most laboratory-scale studies with known chemical components, samples taken from an industrial site are expected to have significantly more complex chemical compositions. Such complexity is likely to cause extra uncertainties in the analysis results when routine analytical protocols are adopted. Therefore, in the present study, additional measures were taken to evaluate and minimize the uncertainties during the analysis.

### Wavelength Scans

Before quantitative EPMA analysis, a full spectrometer wavelength scan was performed on the observed phases in selected samples. This step is essential for samples with complex chemistry for a number of reasons:

1. Identifying all the major and minor elements at level above 0.1 wt.% in the phase of interest. Missing elements at level above 0.1 wt.% in the subsequent quantitative analysis would impact on the analysis quality control, i.e., low analytical totals, and potentially cause erroneous matrix corrections in quantification.
2. Assisting selection of appropriate characteristic x-rays to be measured, identification and evaluation of potential spectral interferences, and developing necessary correction strategy
3. Assisting the development of background correction method for elements to be measured

For example, Fig. 1 shows detailed wavelength scans around Co K emission lines on both slag and matte phase. It can be seen that the characteristic x-rays of Co ( $K_\alpha$  and  $K_\beta$ ) fall between the emission lines of other transition metals occurring at much higher concentrations in the sample. For the slag phase, although the Co  $K_\alpha$  line is more intense compared with the  $K_\beta$  line, it suffers from strong interference from the Fe  $K_\beta$  line. Therefore, Co  $K_\beta$  was selected for the analysis despite the need for a much longer counting time to obtain the necessary detection limit and statistically reliable results. On the other hand, Co  $K_\alpha$  was selected for analysis in the matte phase as the level of interference of Co  $K_\beta$  line by Cu  $K_\alpha$  is much higher.

### Detection Limit and Beam Damage

The detection limit of an element in EPMA is affected by many factors, among which accelerating voltage, beam current, and background counting time can be easily adjusted.<sup>6</sup> Figure 2 shows how the beam current and background counting time affect the detection limit of Ni in the slag phase at fixed electron accelerating voltage. It can be seen

that a detection limit of a few ppm level is achievable for Ni within a reasonable timeframe by using a significantly elevated probe current. However, despite the fact that EPMA is usually promoted as a nondestructive analytical method, extra care needs to be taken when adopting extreme analytical conditions. Figure 3 shows the Ni  $K_\alpha$  counting rates at different beam currents over an analysis period of 300 s. It can be seen that the count rate of Ni  $K_\alpha$  on the slag phase increases in proportion to the beam current and remains constant within the whole analysis period when using all three beam currents tested. In contrast, the count rate of Ni on matte phase drops significantly within the first few seconds after exposure to a beam current of 500 nA, indicating severe beam damage. In the present study, a suitable set of analytical parameters was chosen and the characteristic x-ray counts of measured elements were monitored throughout the analytical session to ensure no obvious error was found caused by beam damage using selected analytical conditions.

### LA-ICP-MS

A selection of trace elements in the samples collected were determined by LA-ICP-MS at the

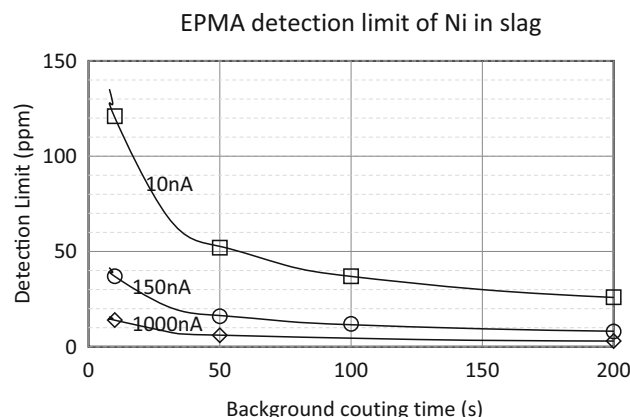


Fig. 2. Factors affecting detection limit of Ni in slag phase at 20 kV acceleration voltage.

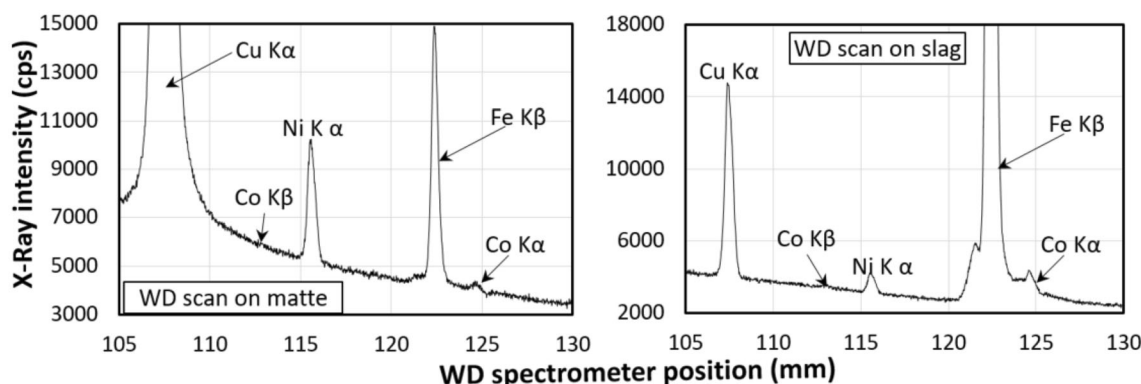


Fig. 1. WD scans of characteristic x-rays of Co ( $K_\alpha$  and  $K_\beta$ ) on slag and matte phase.

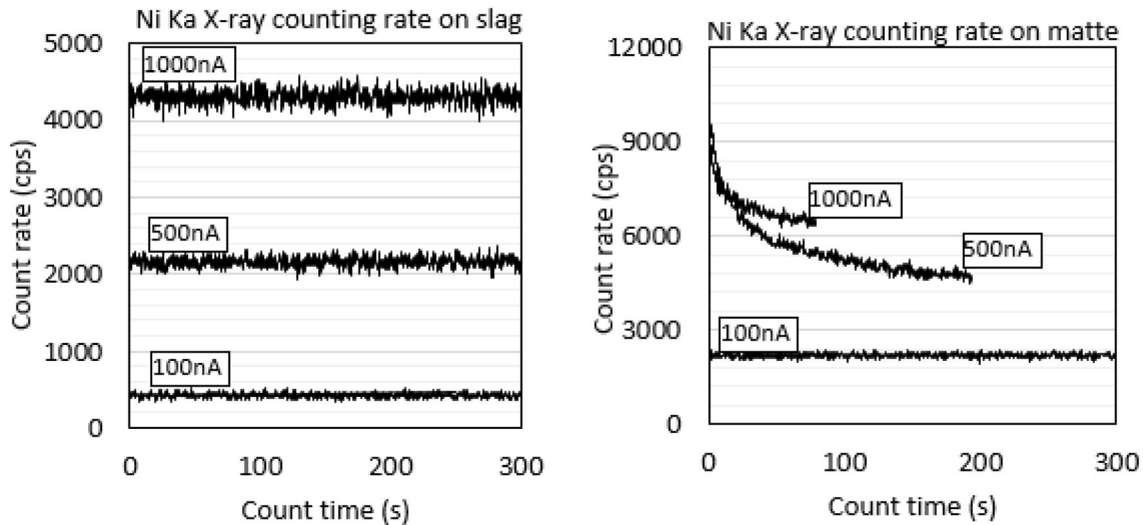


Fig. 3. Effect of beam current on stability of Ni in slag and matte phase.

Research School of Earth Sciences, ANU using an Agilent Technologies 7700 ICP-MS coupled to an ANU HeLEX laser-ablation system with a 193-nm-wavelength EXCIMER laser (110 (ArF) COMPex, Lambda Physik) following the method of Jenner and O'Neill<sup>7</sup>. The elements determined and the isotopes used for these determinations were <sup>59</sup>Co, <sup>60</sup>Ni, <sup>66</sup>Zn, <sup>75</sup>As, <sup>69</sup>Ga, <sup>70</sup>Ge, <sup>78</sup>Se, <sup>113</sup>In, <sup>118</sup>Sn, <sup>121</sup>Sb, <sup>207</sup>Pb, and <sup>209</sup>Bi. Data acquisition involved a 30-s background measurement followed by 30 s of ablation, with a 10 Hz repetition rate. The laser spot size was 82  $\mu\text{m}$ . Si and S concentrations determined by EPMA were used as internal standards, and NIST SRM 610<sup>8</sup>, USGS MASS-1, IMER-3, and a sulfide glass containing Ga and Ge were used as external reference standards. The latter standard was supplied by Allan Pring from Flinders University; its element concentrations are presented in Supplementary Table S3. Unknowns were bracketed by analyses of reference standards every five to ten analyses, to correct for instrument drift. Data were processed using the Iolite v3.1 software package.<sup>9</sup> The element detection limits obtained are reported in Supplementary Table S4.

## RESULTS AND DISCUSSION

### Microstructural Analysis

Typical microstructures of selected samples are presented in a set of SEM micrographs in Fig. 4A–F. As can be seen from the sample overview in Fig. 4A, the sample consisted of spinel and matte phases suspended in a slag matrix. Despite the fact that the received samples were collected by quenching directly into water at room temperature, recrystallization/precipitation of secondary phases was still observed in the slag phase. It is therefore critical to distinguish the primary phases (stable at high temperature) from those formed upon quenching prior to quantitative analysis.

### Slag Phase

As can be seen from Fig. 4B, which shows a magnified microstructure of Fig. 4A, the slag phase immediately adjacent to the surface of the sample particle was generally found to be preserved best as it is expected to come into direct contact with water first and quench at the highest rate. Even so, very fine precipitates ( $\sim 100$  nm) of Cu-S-rich particles from the slag phase can be seen at high magnification, with a spatially random distribution indicative of precipitation during quenching. More precipitation and coarser precipitates from the slag phase were observed when moving further into the center of the sample, presumably due to slower cooling, as shown in Fig. 4C, D.

### Matte Phase

Unlike the slag phase, the entrained matte phase recrystallized more readily upon quenching. Some minor elements exsolved from the sulfide matrix, and segregated to form metal-rich veins (Fig. 5). Therefore, more points were analyzed in the matte phase to reduce the chance of nonrepresentative sampling. The entrained matte and precipitated Cu-S-rich particles from the slag phase can normally be identified without too much difficulty: the precipitated sulfide particles from the slag phase during cooling were usually less than 10  $\mu\text{m}$ , while entrained matte droplets were typically from 10  $\mu\text{m}$  to a couple of millimeters in diameter, as shown by Fig. 4E.

### Spinel Phase

The primary spinel crystals in the slag samples were often found to have a euhedral shape, with typical sizes ranging from 10  $\mu\text{m}$  to 50  $\mu\text{m}$ , while the recrystallized spinel phase usually exhibited dendritic structure with size less than 5  $\mu\text{m}$ , as shown



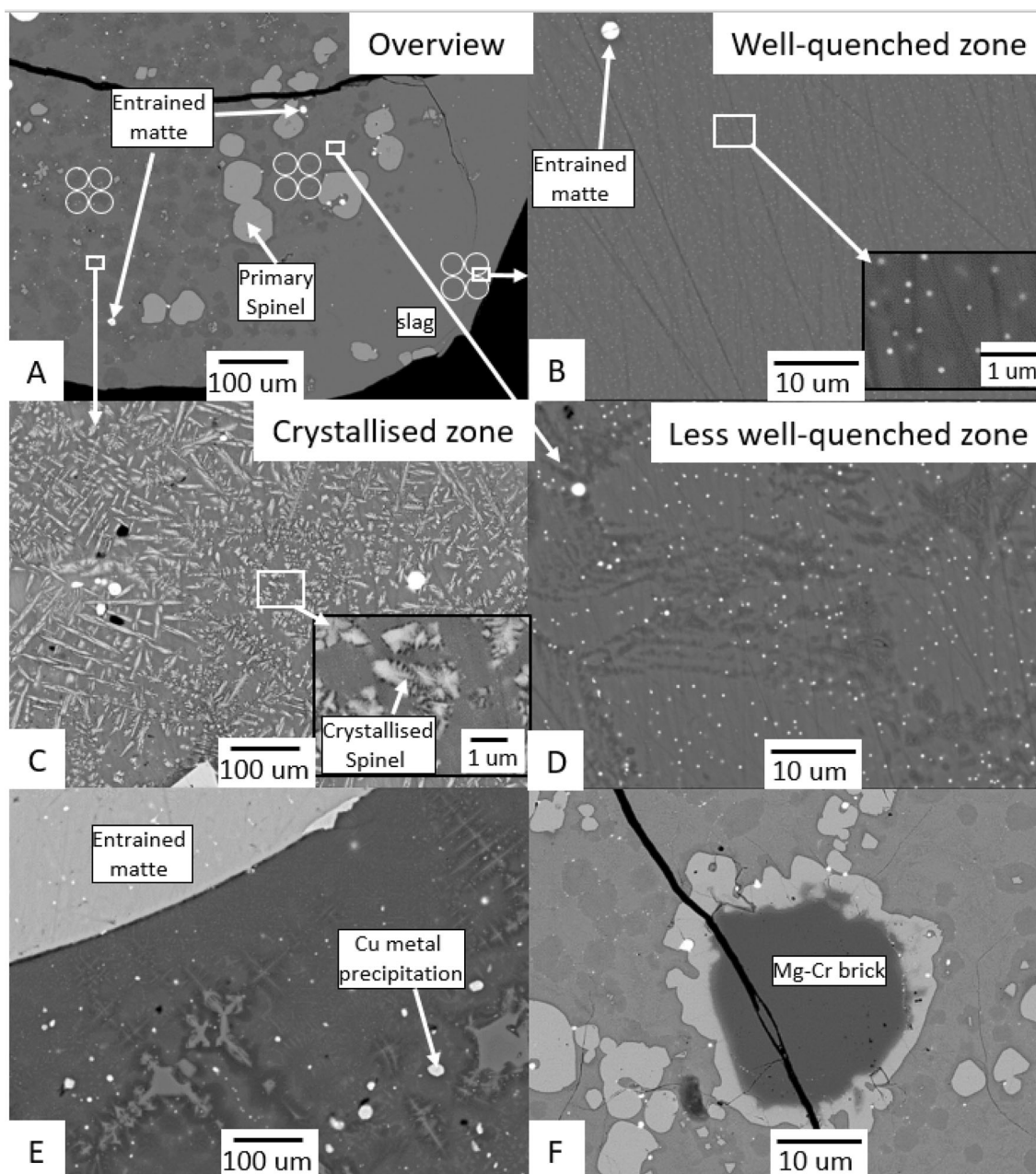


Fig. 4. Typical microstructures of copper converting samples.

in Fig. 4C. Occasionally, spinel particles with a core having high Cr and Mg were observed (Fig. 4F). They generally appear darker compared with primary spinels under SEM in backscattered electron mode and are likely relics of refractory materials entrained by slag erosion.

In the present study, the primary phases (that is, those stable at high temperature) in the samples were all clearly identified before quantitative measurements were carried out.

## Measurement Uncertainties

### EPMA

To account for the submicron-scale heterogeneity observed in the slag and matte phase, analyses were made with a defocused electron beam of  $30\ \mu\text{m}$  in the areas of the samples where quenching was deemed to be most effective. Such approach has been controversial because the matrix correction procedure in EPMA analysis assumes the sampling volume is homogeneous. Barkman et al.<sup>10</sup> measured

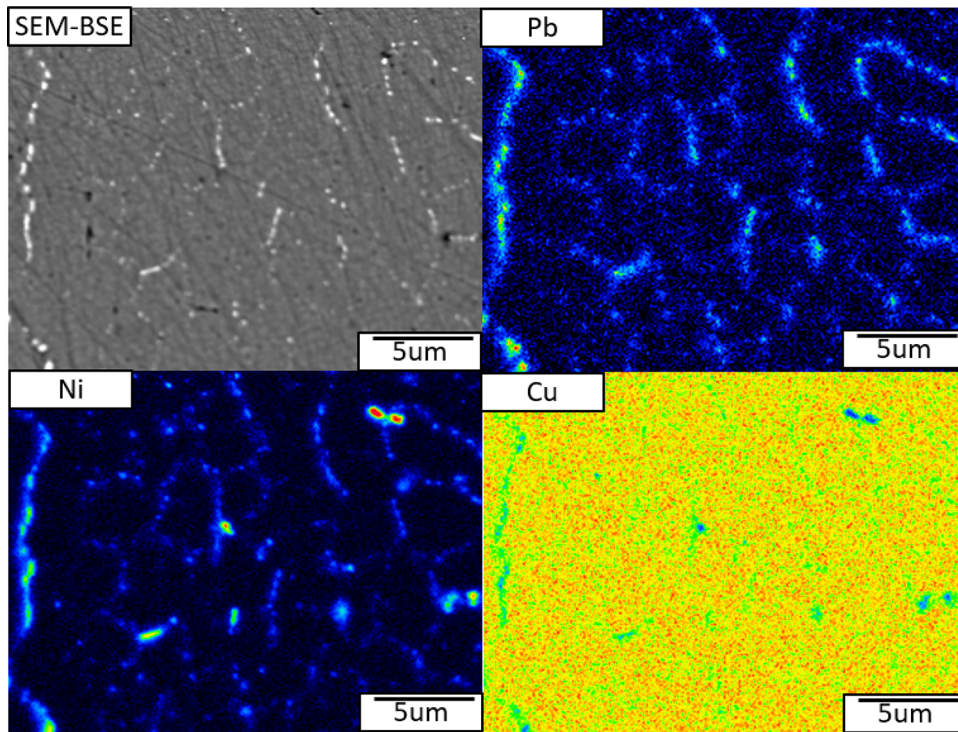


Fig. 5. Detailed microstructure of entrained matte phase and selected elemental mapping by WDS.

the average composition of a region of interest in a natural silicate rock using different electron beam sizes. They reported up to 6% error for Mg, Al, and Gd when using a defocused beam. By contrast, Fallah et al.<sup>11</sup> measured the Cu concentration in slag samples with finely precipitated Cu-rich particles from gas/slag/matte/tridymite phase equilibrium experiments using EPMA with different beam sizes. The authors observed improved analysis precision, while the analysis accuracy was not affected when using larger beam sizes.

This potential source of error was evaluated by measuring the areas of slag phase with different extents of quench crystallization. White circles labeled A1 to A3 in Fig. 4A show where the measurements were performed. The average minor element concentrations of four analysis spots are reported in Supplementary Table S5 with their relative standard deviations. It can be seen that, for all measured minor elements, the results from all three areas agree well, suggesting that the potential error in minor element concentration measurement in slag phase due to heterogeneity within the sampling volume is negligible.

#### LA-ICP-MS

The sampling depth of LA-ICP-MS analysis is typically around 30  $\mu\text{m}$ , as opposed to 1  $\mu\text{m}$  to 3  $\mu\text{m}$  for EPMA. This adds to the possibility of error due to the increased chance of sampling inclusions of another phase beneath the sample surface.

Figure 6a shows a  $\sim 25\text{-}\mu\text{m}$ -deep pit formed in the slag phase after 30 s of ablation using a beam size of 80  $\mu\text{m}$ . An entrained matte particle at the bottom of the pit can be seen exposed, indicating that part of it was sampled/analyzed during the analysis of the slag phase. Figure 6b shows a raw time-resolved LA-ICP-MS downhole spectra of an analysis spot on the slag phase. Two obvious “spikes” on the  $^{63}\text{Cu}$  and  $^{60}\text{Ni}$  signals occur coincident in time during ablation, suggesting the presence of an inclusion of matte phase within the sampled volume. It is an advantage of LA-ICP-MS that this type of error can be identified by examination of time-resolved ablation spectra, allowing their effects to be minimized by removing the affected time segments for these elements.

Another source of error comes from not using matrix-matched standards. This is a particular concern for measuring the matte phase. It has been well documented that sulfides ablate very differently from oxide minerals/glasses during laser ablation, thus the use of commercially available silicate standards could cause significant systematic errors in sulfide analyses.<sup>12,13</sup> In present study,  $\sim 10\%$  difference was observed between the analyses results for some elements when using two different sulfide standards (Supplementary Fig. S1). To resolve the discrepancies, further development of matrix-matched sulfide standards for copper matte analysis is needed.

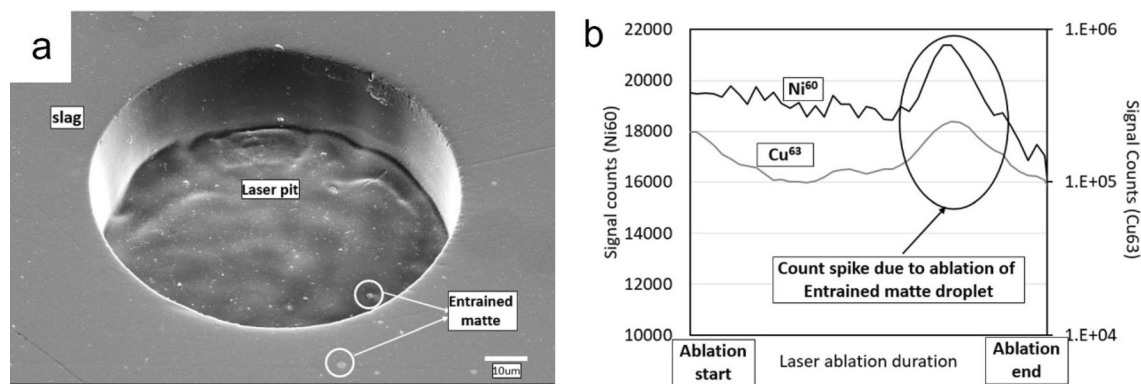


Fig. 6. (a) Ablation crater in slag phase; (b) LA-ICP-MS time-resolved intensity showing count spikes for Cu<sup>63</sup> and Ni<sup>60</sup>.

### Minor Element Concentrations in Slag, Matte, and Spinel Phases

A total of 15 elements in the slag, matte, and spinel phase were measured by EPMA and LA-ICP-MS and are reported with their respective standard deviations in Supplementary Table S6. The concentrations of Pb, Co, Ni, Sn, Sb, and As in the slag phase analyzed by EPMA are compared with the analyses by LA-ICP-MS in Supplementary Fig. S2. The results for Pb, Co, and Ni are in excellent agreement over the entire range of relevant concentrations, lying between ~ 500 ppm and 25,000 ppm. The concentration of Sn, Sb, and As measured by LA-ICP-MS appears to be consistently higher than that obtained by EPMA. This difference could be due to the limitations of the linear interpolation background correction method applied in the present EPMA analyses. An example is shown in Supplementary Fig. 3, where the background intensity of Sn L<sub>α</sub> line was determined by linear interpolating background intensity at spectrometer positions corresponding to a lower (point B) and higher energy (point A) than the characteristic x-ray. This method overestimated the background intensity in this specific case because the background is curved, leading to the measured net intensity for Sn being lower than the true net intensity. More sophisticated background determination methods including exponential and multi-point polynomial fitting may improve the analysis accuracy, but these have not been tested in the present study due to the lack of supporting software.

### Distribution Coefficients

The distribution coefficients,  $L$ , of the minor elements were calculated using Eq. 1,

$$L_{\text{element}i}(\text{phase A/phase B}) = \frac{\text{wt\% element } i \text{ in phase A}}{\text{wt\% element } i \text{ in phase B}} \quad (1)$$

The average values obtained from the EPMA and LA-ICP-MS analyses were used for the calculation wherever possible.

### Distribution of Minor Elements Between Slag and Matte Phase

The distribution coefficients of Pb, Zn, Co, Sn, Sb, As, Ni, Bi, Se, and In between slag and the matte phase are plotted against matte grade (wt.% Cu in matte phase) together with literature data in Fig. 7. With increasing matte grade, the distribution coefficients of Pb, Zn, Co, Sn, Ni, Bi, and In between slag and matte were found to increase, with the largest changes being observed at matte grades above 75 wt.%. These results are in good agreement with recent laboratory studies by Shishin et al.<sup>3,5</sup> and Sukhomlinov et al.<sup>14</sup> despite the fact that those were conducted at silica saturation. The difference in results becomes more noticeable at high matte grade, which may be due to some replacement of Cu in the matte phase in the industry samples by Pb, Zn, and Ni, thus decreasing the amount of Cu in the matte phase compared with that in stoichiometric Cu<sub>2</sub>S. By contrast, the distribution coefficient of Sb, As, and Se reduces with increase of matte grade. The distribution coefficient of Sb was consistent with that reported by Shinshin et al., but significantly higher than reported by Yazawa et al.<sup>15</sup> or Roghani et al.<sup>16</sup> However, As was found to show higher affinity to the matte phase than measured by Shinshin et al.<sup>5</sup> For Se, the present study shows that it strongly partitions into the matte phase, which is consistent with the findings of Desai et al.<sup>17</sup> It was suggested that, at high matte grade, Se dissolved in the matte phase oxidized to form SeO<sub>2</sub>, which was expected to enter the gas phase. Excellent agreement was found between the present study and Sukhomlinov et al.<sup>14</sup> in terms of the In distribution behavior between slag and matte.



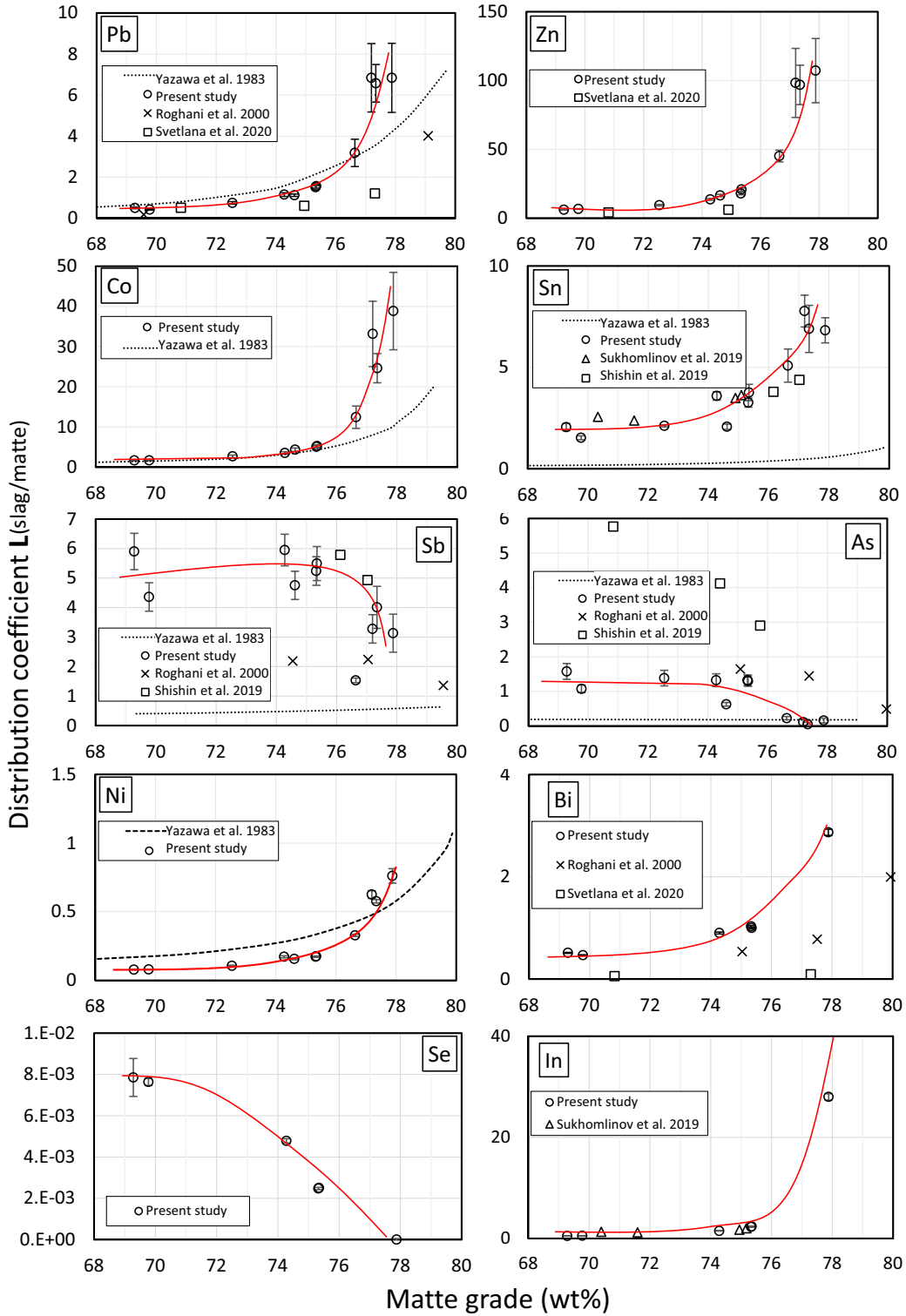


Fig. 7. Comparison of minor element distribution between slag and matte phase determined by present study with literature data from Yazawa et al.<sup>15</sup> at 1300°C and 0.1 atm SO<sub>2</sub>, Roghani et al.<sup>16</sup> at 1300°C and 1 atm SO<sub>2</sub> with MgO saturation, Shishin et al.<sup>3</sup> at 1200°C and 0.14 atm to 0.24 atm SO<sub>2</sub> with SiO<sub>2</sub> saturation, Shishin et al.<sup>5</sup> at 1200°C and 0.1 atm to 0.3 atm SO<sub>2</sub> with SiO<sub>2</sub> saturation, Sukhomlinov et al.<sup>14</sup> at 1300°C and 0.1 atm SO<sub>2</sub> with SiO<sub>2</sub> saturation, and Svetlana et al.<sup>20</sup> at 1200°C and 0.1 atm to 0.3 atm SO<sub>2</sub> with SiO<sub>2</sub> saturation. Red solid lines are trend lines for the present study; error bars (2 $\sigma$ ) calculated based on standard deviations of measured concentrations of corresponding elements (Color figure online).



### Distribution of Minor Elements Between Spinel and Matte Phase

Since many current Cu smelting/converting processes are operated at temperatures below the liquidus of the slag, spinel phases are commonly found, and sometimes constitute a large proportion of the discarded slag materials. Despite the fact that the spinel phase is capable of hosting significant amounts of 2+ or/and 3+ metal cations, which ultimately affects the deportment of some of the minor elements, it is often overlooked and systematic investigations of its chemical compositions have been few. Klemettinen et al.<sup>18</sup> experimentally studied the equilibrium distribution of trace level of Ni between iron aluminum silicate slag, Cu metal, and iron aluminum spinel phase at 1300°C under oxygen partial pressures between  $10^{-10}$  atm and  $10^{-4}$  atm; the authors found that the nickel concentration increased with increase of the oxygen partial pressure. Later, a similar equilibrium study with MgO addition by Dańczak et al.<sup>19</sup> also reported an increased Ni concentration in the spinel phase when the oxygen partial pressure was increased from  $10^{-11}$  atm to  $10^{-8}$  atm. The distribution coefficients of minor elements between spinel and matte measured in the present study are plotted against the matte grade in Fig. 8. The distribution coefficients of Ni, Zn, and Co between spinel and matte show similar trends to those between slag and matte, increasing with higher matte grade. Ni preferentially enters the matte phase over the slag phase throughout the matte grades investigated, with the spinel phase taking up more Ni than the matte phase at matte grade above 75 wt.%. The effect of matte grade on the distribution coefficient of Sn between spinel and

matte does not show a clear trend due to larger standard deviation of the Sn concentration in the spinel phase, but Sn concentrations in the spinel phase were at least five times higher than in the matte phase for all samples.

### Advantages and Limitations of Chemical Assay by Microanalysis Methods

Controlled laboratory equilibrium studies provide fundamental information on the effects of process conditions on the distribution behavior of minor elements. However, the important factors affecting the process output include that the reaction kinetics and complex feed compositions that are particular to a specific operation are generally not taken into account. Moreover, developing experimental techniques to study systems with volatile species has proven challenging, limiting the relevance or applicability of small-scale laboratory studies.

Analyzing samples taken directly from smelting/converting/refining processes using microanalytical techniques reveals the elemental distributions between phases under the actual process conditions. Combined with other routine on-site measurements such as process temperature and bulk chemical assay of slag/matte/metal/off-gas, it can provide quantitative information on not only the process mass balance but also the mechanisms by which valuable elements are lost in discarded slag material. Furthermore, the distribution behavior of minor elements of potential economic interest in the future can be followed through the process flow, even at trace level ( $\sim 1$  ppm). This information is central to future process optimization and development.

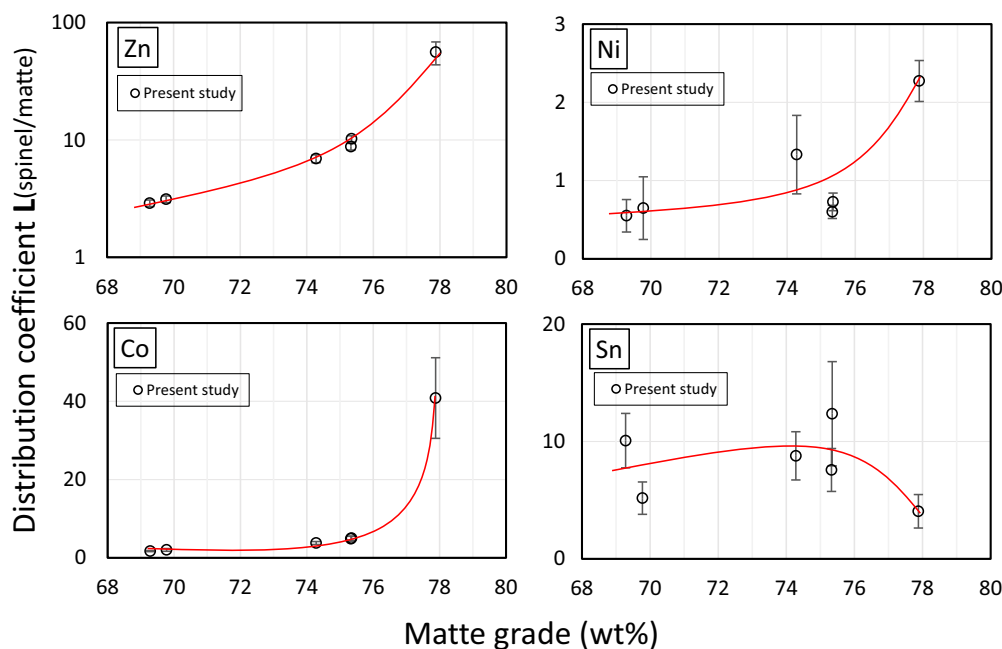


Fig. 8. Minor element distribution between spinel and matte phase determined in present study. Red solid lines are trend lines for the present study; error bars ( $2\sigma$ ) calculated based on standard deviations of measured concentrations of corresponding elements (Color figure online).

The successful application of microanalysis techniques on industry samples depends heavily on developing sampling strategies to ensure that the samples taken for analysis are representative, and that their mineralogy and microstructures after quenching can be related to those obtaining at the high-temperature conditions of the process. At present, the lack of well-characterized sulfide and metal standard materials for LA-ICP-MS in particular limits the accuracy of microanalysis of trace elements in sulfide and metal phases.

### CONCLUSION

A quantitative microanalysis method using EPMA and LA-ICP-MS has been developed to measure minor element concentrations in complex copper converting slag samples taken from an industrial site. It was demonstrated that, by avoiding contamination from mixing of phases, accurate and precise minor element distributions between slag, matte, and spinel phase can be obtained using microanalysis techniques by direct measurement of representative plant samples.

It was also found in the present study that, although LA-ICP-MS is capable of measuring elements at sub-ppm levels, its analysis accuracy heavily relies on the use of matrix-matching standards. Future development of matrix-matching standards, particularly for matte, speiss, and metal, is essential to extend the application of LA-ICP-MS in metallurgy research.

### ACKNOWLEDGEMENTS

The authors thank Dr. Denis Shishin for valuable discussion and the anonymous reviewers for constructive comments. The authors acknowledge the facilities of Microscopy Australia at the Centre for Advanced Microscopy, Australian National University, a facility that is funded by the university and the Federal Government.

### CONFLICT OF INTEREST

On behalf of all authors, the corresponding author states that there are no conflicts of interest.

## SUPPLEMENTARY INFORMATION

The online version contains supplementary material available at <https://doi.org/10.1007/s11837-021-04920-7>.

### REFERENCES

1. S.E. Jackson, H.P. Longrich, G.R. Dunning, and B.J. Freyer, *Can. Mineral.* 30, 1049. (1992).
2. K. Avarmaa, H. O'Brien, H. Johto, and P. Taskinen, *J. Sustain. Met.* 1, 216. (2015).
3. D. Shishin, T. Hidayat, J. Chen, P.C. Hayes, and E. Jak, *Calphad* 65, 16. (2019).
4. D. Shishin, T. Hidayat, J. Chen, P.C. Hayes, and E. Jak, *J. Sustain. Met.* 5, 240. (2019).
5. D. Shishin, T. Hidayat, J. Chen, P.C. Hayes, and E. Jak, *J. Chem. Thermodyn.* 135, 175. (2019).
6. T.O. Ziebold, *Anal. Chem.* 39, 858. (1967).
7. F.E. Jenner, H.S.C. O'Neill, *Geochem. Geophys. Geosyst.*, 13, (2012).
8. K.P. Jochum, U. Weis, B. Stoll, D. Kuzmin, Q. Yang, I. Raczek, D.E. Jacob, A. Stracke, K. Birbaum, and D.A. Frick, *Geostand. Geoanal. Res.* 35, 397. (2011).
9. C. Paton, J. Hellstrom, B. Paul, J. Woodhead, and J. Hergt, *J. Anal. At. Spectrom.* 26, 2508. (2011).
10. J.E. Barkman, P. Carpenter, J.-C. Zhao, and J.J. Donovan, *Microsc. Microanal.* 19, 848. (2013).
11. A. Fallah-Mehrjardi, T. Hidayat, P.C. Hayes, and E. Jak, *Metall. Mater. Trans. B* 48, 3002. (2017).
12. P.J. Sylvester Laser-ablation-ICPMS in the earth sciences: principles and applications, vol 29. Mineralogical association of Canada, (2001).
13. L. Danyushevsky, P. Robinson, S. Gilbert, M. Norman, R. Large, P. McGoldrick, and M. Shelley, *Geochem. Explor. Environ. Anal.* 11, 51. (2011).
14. D. Sukhomlinov, L. Klemettinen, H. O'Brien, P. Taskinen, and A. Jokilaakso, *Metall. Mater. Trans. B* 50, 2723. (2019).
15. A. Yazawa, S. Nakazawa, and Y. Takeda, *Paper Present. Adv. Sulfide Smelt.* 1, 99. (1983).
16. G. Roghani, Y. Takeda, and K. Itagaki, *Metall. Mater. Trans. B* 31, 705. (2000).
17. B. Desai, V. Tathavadkar, and S. Basu, *Metall. Mater. Trans. B* 49, 1213. (2018).
18. L. Klemettinen, K. Avarmaa, P. Taskinen, A. Jokilaakso. Behavior of nickel as a trace element and time-dependent formation of spinels in WEEE smelting. In: *Extraction 2018*. Springer, pp. 1073-1082.
19. A. Dańczak, L. Klemettinen, H. O'Brien, P. Taskinen, D. Lindberg, and A. Jokilaakso, *J. Sustain. Met.* 7, 1. (2021).
20. S. Sineva, M. Shevchenko, D. Shishin, T. Hidayat, J. Chen, P.C. Hayes, and E. Jak, *JOM* 72, 3401. (2020).

**Publisher's Note** Springer Nature remains neutral with regard to jurisdictional claims in published maps and institutional affiliations.